Pres. 41st Advanced ICFA Beam Dynamics Workshop on Energy Recovery Linacs - "EROL7", 21-25 May 2007, Daresbury, U.K.

BNL-78118-2007-CP

STATUS OF DIAMOND SECONDARY EMISSION ENHANCED PHOTOCATHODE*

T. Rao, I. Ben-Zvi, X. Chang, J. Grimes, R. Grover,
A. Isakovic, **J. Smedley**, R. Todd, **J. Warren**, and Q. Wu
Brookhaven National Laboratory, Upton, NY 11973-5000

J. Bohon
Case Western Reserve University, Cleveland, OH

D. Fischer
NIST, Gaithersburg, MD

D. Dimitrov
Tech-X, Boulder, CO

May, 2007

DISCLAIMER

STATUS OF DIAMOND SECONDARY EMISSION ENHANCED PHOTOCATHODE*

T. Rao, I. Ben-Zvi, X. Chang, J. Grimes, R. Grover, A. Isakovic, J. Smedley, R. Todd, J. Warren, Q. Wu, Brookhaven National Laboratory, NY, USA
J. Bohon, Case Western Reserve University, Cleveland, OH, USA, D. Fischer, NIST, Gaithersburg, MD, USA, D. Dimitrov, Tech-X, Boulder, CO, U.S.A.

Abstract

The diamond secondary emission enhanced photocathode (SEEP) provides an attractive alternative for simple photo cathodes in high average current electron injectors. It reduces the laser power required to drive the cathode, simultaneously isolating the cathode and the RF cavity from each other, thereby protecting them from contamination and increasing their life time. In this paper, we present the latest results on the secondary electron yield using pulsed thermionic and photo cathodes as primary electron sources, shaping the diamond using laser ablation and reactive ion etching as well as the theoretical underpinning of secondary electron generation and preliminary results of modeling.

INTRODUCTION

In the recent years, there has been considerable interest in generating high brightness electron beams with average currents in the range of 1 mA to 1A for FEL, light source and ion cooling applications [1-3]. Direct generation of such high currents from photo cathodes requires highly efficient cathodes as well as very powerful lasers. Even then, there is a concern that the vacuum degradation that can result from such high current could reduce the life time of these sensitive cathodes to impractical levels. Furthermore, in the case of SRF injectors, the cathodes may also contaminate the cavity, reducing their performance level. In order to alleviate these problems, use of a secondary emitter that will amplify the primary current while acting as a barrier between the primary cathode and the cavity has been proposed [4]. Synthetic diamond has been shown to have secondary electron yield (SEY) exceeding 100 [5]. The electrical, mechanical and thermal properties of diamond also make it an ideal candidate for this application. In this paper we present the SEY measured using primary electrons from a pulsed thermionic cathode as well as a pulsed photo cathode for the first time.

Operating the SEEP inside a high average current, high frequency RF injector mandates the use of a large aspect ratio diamond (1 cm x 30 μm) than is commercially available. In order to thin the diamond to the required dimensions, the commercial synthetic diamond has been etched using two different techniques: RIE and laser ablation. The surface morphology before and after processing has been presented in the paper. Preliminary results from simulations of the generation and transport of secondary electrons are also presented.

MEASUREMENTS OF SEY: PULSED THERMIONIC GUN

The experimental arrangement for measuring the SEY using a pulsed thermionic gun is shown in Figure 1. The primary electrons are generated in a commercial thermionic gun. The pulse duration of the electron beam can be varied from DC to 20 ns using blanking and capacitive pulsing. The current can be varied from 10 nA to 1 mA with a the suitable firing unit. Deflection and focusing elements in the gun provide necessary beam handling capability. The focal spot size of the primary electron beam depends critically on its energy and the current.

The transmission mode experiment setup is schematically shown in figure 1. The primary electrons penetrate the metal coating with some energy loss depending on the metal coating thickness and generate electron-hole pairs in diamond. The electron-hole pairs are separated by the electric field and the electrons drift through diamond and generate the current signal.

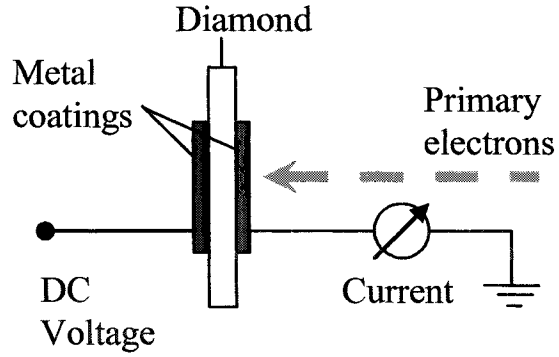

Figure 1 Schematic of the experimental arrangement for measuring gain with a pulsed thermionic electron gun as the primary source

For these measurements, both faces of a polycrystalline sample of 10 mm diameter and 0.15 mm thickness were coated with 20 nm Ti and 20 nm of Pt. A Primary charge pulse of 610 nA, with a pulse length of 6 μs and energy of 6 keV incidents on one of the faces at a repetition rate of 10 Hz. The secondary current is measured as a function of the field across the diamond and the gain is plotted in Figure 2.

In the absence of trapping, the measured gain is the difference between the electron-hole pair generated by the primary and the electron-hole pair lost due to recombination. This can be modeled by assuming that the

recombination rate is proportional to the product of the electron density and the hole density. The electron and hole drift velocity v_d as a function of the electric field can be expressed as [6]:

$$v_d = \frac{\mu_0 F}{\left[1+\left(\mu_0 F / v_s\right)^{\gamma}\right]^{1/\gamma}}$$

where $\mu_0 = 2000 cm^2/Vs$ is the mobility at low field and is assumed to be the same for both electrons and holes. F is the electric field, $v_s = 1.1 \times 10^5 m/s$ is the saturation drift velocity and $\gamma = 1$ is the fitting parameter. Electron propagation through the diamond and the gain under different applied fields were calculated iteratively and are shown in Figure 2. As can be seen by the overlap between the experimentally measured and theoretically calculated gains, this model describes the dependence of gain on the field quite accurately.

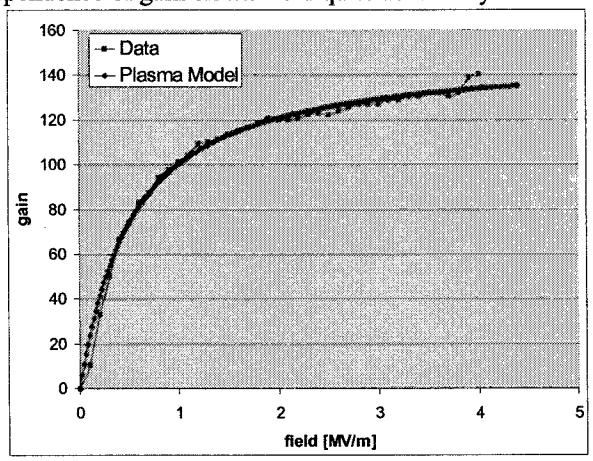

Figure 2 Gain in transmission mode and simulation results based on electron-hole separation in the presence of the field.

MEASUREMENTS OF SEY: PHOTOELECTRIC GUN

The SEEP in an RF injector is in the form of a capsule consisting of a primary electron source and a diamond secondary emitter that is electrically isolated from the primary source. The surface of the diamond facing the cathode is metalized to provide the replacement current and the surface facing the RF cavity is specially treated to reduce the electron affinity of the diamond. An electric field is applied between the primary source and the diamond so that the primary electrons can be accelerated to the required energy. The RF field in the cavity penetrates into the diamond, transporting the secondary electrons to the front surface of the diamond where they are released in to the cavity.

For the following measurements, the diamond and the photocathode were assembled to mimic closely the capsule that would be installed in the SRF injector application.

Diamond preparation:

A polycrystalline, electronic grade diamond sample (Harris International Diafilm El) of 10 mm diameter and 0.3 mm thickness was etched chemically to remove organic, metal and non-diamond carbon contaminants. One of the faces was metalized by sputtering ~ 20 nm each of Ti and Pt. The sample was then installed in an ultrahigh vacuum cell, heated to 450 C, cooled to room temperature, and the uncoated surface is hydrogenated by exposing it to 10^{-6} torr of molecular hydrogen in the presence of a hot W filament. Subsequently, a five layer stack containing the diamond, Ticusil (braze material), a Nb washer, Ticusil, and a sapphire washer was placed in a vacuum furnace heated to 900 C to produce a brazed stack of sapphire, Nb and diamond that forms one side of the capsule (See figure 3).

Photocathode preparation:

The photocathode material used for these measurements is oxygen free copper that was machined, cleaned with acetone and acetic acid to remove oil and oxide layers, mechanically polished with up to 1 micron diamond polishing compound, cleaned in hexane ultrasonic bath, dried with a nitrogen gas jet and inserted into the vacuum system.

Experimental arrangement:

Both the photocathode and the diamond stack are inserted into an ultrahigh vacuum chamber held at ~10^{-9} Torr. The photocathode and the diamond stack were sealed together by a thin indium wire to form the secondary emitter capsule. For some measurements, the diamond stack was brought in contact with the photocathode without actually sealing the two for ease of operation. A metal mesh in front of the diamond was used as the anode. Both the photocathode and the anode were connected to high voltage (up to – 5 kV on the photocathode and + 5 kV on the anode) while the Nb layer on the diamond stack was used to measure the primary electrons arriving and secondary electrons leaving the diamond. A schematic of the experimental layout is shown in Figure 3.

The UV light used to generate the primary photoelectrons was produced by a Xe flash lamp with a 5 J bulb. The light from the lamp passes through the wire mesh, diamond, and partially-transmitting metal layer on the diamond and incidents on the photocathode. In order to eliminate photoemission from the diamond, the UV wavelengths above the diamond band gap were blocked by inserting another piece of polycrystalline diamond in the optical path before the vacuum cell.

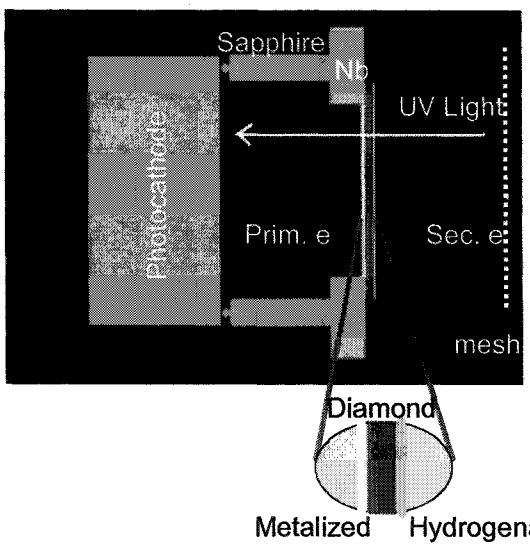

Figure 3 Schematic of the experimental arrangement for measuring gain with photo electrons as the primary source

The primary charge Q_p arriving at the diamond is measured by biasing the photocathode to -2.5 kV, the aanode to 0 and integrating the signal from the Nb using an oscilloscope. The charge leaving the diamond Q_e was measured similarly, but with an anode bias of 1.25 kV at a diamond to anode distance of 0.5 mm. The secondary charge Q_s can be calculated as $Q_s = Q_e + Q_p$. The primary and secondary signals and a corresponding gain of ~ 1.5 are shown in Figure 4.

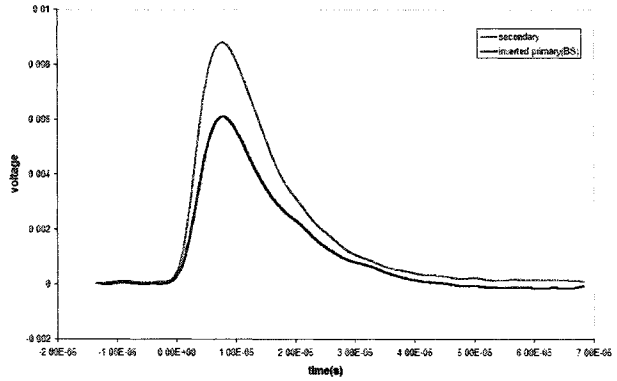

Figure 4 Signals from 12.8 nC primary charge, 20 nC secondary charge and corresponding gain of 1.5 in the capsule mode.

Gain has been measured for the first time with photocathode as the primary electron source with very high primary charge, in a capsule geometry. However, this gain is significantly lower than the gains measured with other arrangements. This low gain could be attributed to a number of process and experimental parameter related factors. The diamond preparation process could have reduced the hydrogenation and increased the Ti diffusion into diamond during the brazing process. The low primary electron energy, especially after energy loss in the passage through metal layer, could also result in lower gain. The lower electric field in the diamond is expected to reduce the velocity of the electrons and increase the probability of recombination.

DIAMOND SHAPING

Laser ablation

The electron beam transport in the diamond mandates that the field inside the diamond has to be > 1 MV/m [6] during the entire transit time of the electrons in the diamond to minimize the electron bunch broadening i.e., the primary electrons enter and the secondary electrons exit the diamond during the positive cycle of the RF field. Furthermore, to generate a low emittance beam, the electrons need to exit the diamond at the correct RF phase, typically at ~ 67° from zero. In order to satisfy these two criteria in a 703 MHz RF injector, the thickness of the diamond has to be < 30 μm. In addition, since the photocathode material in the final capsule would be a multi alkali that needs to be in ultrahigh vacuum, there is a significant pressure differential between the evacuated inside and the ambient outside of the capsule. Hence, the structural integrity of the capsule would benefit by shaping of the diamond with thicker outer edges and a thinner center. Since commercial synthetic diamond sample are flat with thickness in the range of 100 μm or higher, we have started investigating shaping the diamond using laser ablation and reactive ion etching (RIE).

Laser ablation rates of ~17 μm/minute have been achieved using a 248 nm excimer [7]. We have studied ablation of single and poly crystalline diamond at different laser wavelengths, pulse durations, intensities and in the presence of various oxygen concentrations. The oxygen did not affect the ablation process significantly. The dependence on wavelength and pulse duration are summarized in Table 1

Table 1 Summary of ablation results. □is the wavelength of the laser and □is the pulse duration

□ nm	□	ThresholdEnergy	Results
266	~ 20 ps	80μJ	See Fig. 5a
266	~ 10 ns	80μJ	Similar to ps UV, but more surface damage
532	~15 ns	130 μJ	Higher ablation threshold, Large, deep damage, ragged edges, does not mimic scan
1064	~ 20 ns	NA	No ablation even with > 200 μJ

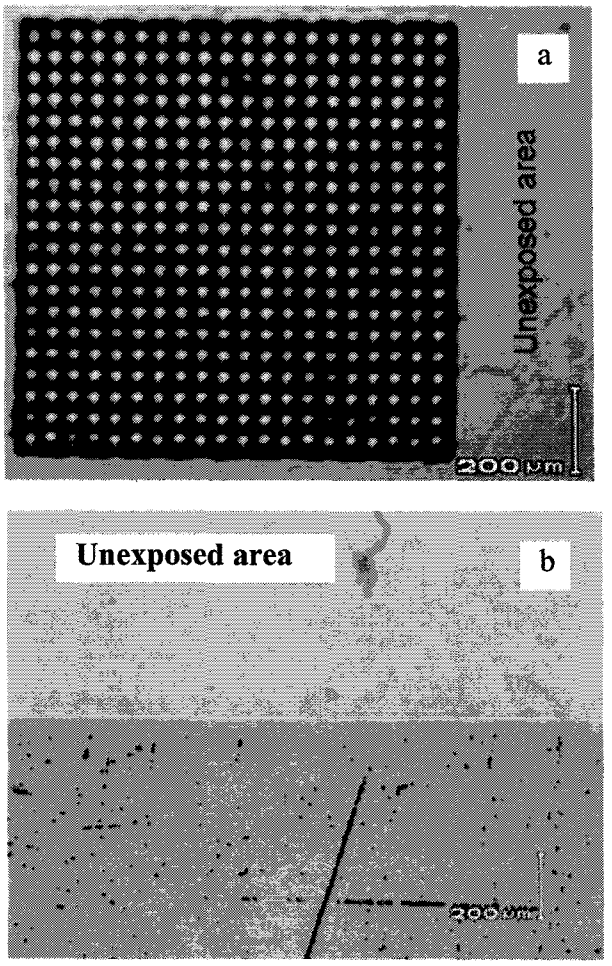

Figure 5 Microscope photographs of a) polycrystalline diamond sample, b) single crystal diamond sample ablated by ps UV laser beam. See text for beam parameters.

Figure 5 shows microscopic photographs of a single crystal(b) and polycrystalline (a) diamond ablated by 266 nm radiation, with ~ 20 ps duration, and 80 μJ energy. For the polycrystalline sample, the laser was raster scanned in both x and y directions 10 times with a scan step of 50 μm for 70 minutes at a repetition rate of 10 Hz. The step size and the number of scans were reduced to 10 μm and 4 times respectively for the single crystal sample, with the total scan time of 10 hrs and the energy was maintained at ~ 100 μJ.

As can be seen from the photographs, the polycrystalline sample reproduced the raster pattern, has a large residue as well as possible cracks along the grain boundaries (see Figure 6 a). NEXAFS analysis of this area indicates that the residue is primarily amorphous carbon. NEXAFS is a highly surface sensitive technique, it can clearly delineate surface impurity from the bulk impurity and can identify different forms of carbon unequivocally. Figure 6 b shows a photograph of the same sample before and after exposure to UV light from a Hg arc lamp (Jelight, GLF-12-SRC) for 6 hrs. The IR transmission (for wave numbers of 800-4000 cm^{-1}) of this area has changed from 65% before the UV radiation to 94% after the radiation, corresponding to a factor of 7 reduction in the thickness of the amorphous carbon layer. Thus UV cleaning can be used to removed amorphous carbon be effectively.

The photograph of the single crystal diamond ablated by the same laser with similar parameters indicates that the ablation process does not leave residue in this sample, no cracking or filamentation is present and the ablated area is smoother.

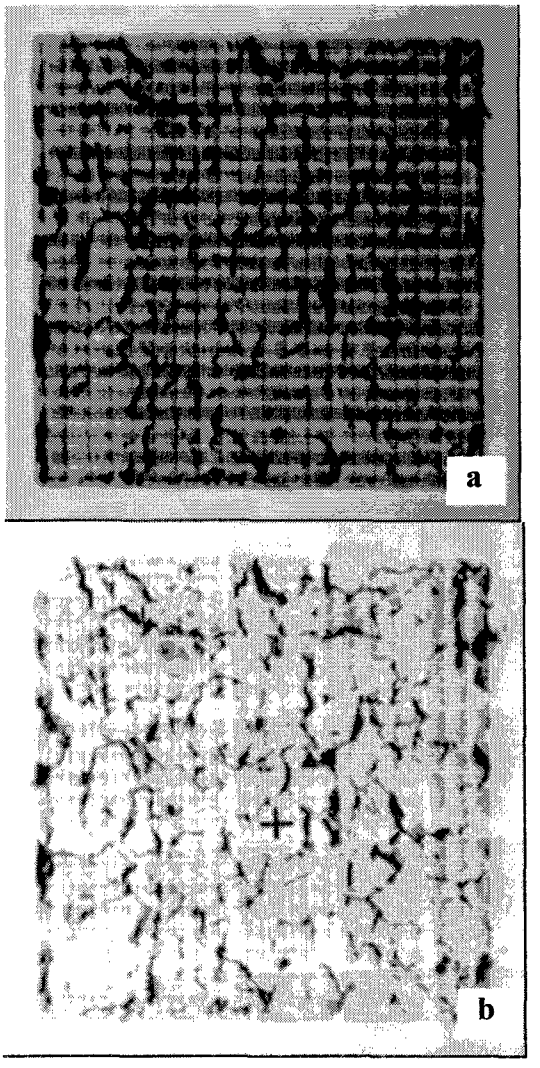

Figure 6 Microscope photograph of polycrystalline sample ablated by ps UV laser beam a) before exposure to UV lamp b) after exposure to UV lamp for 6 hrs

An AFM picture of the ablated polycrystalline sample is shown in Figure 7. It can be seen from the figure that the ablation depth is ~ 1 μm, ablation is deeper in the regions where the x scans and y scans overlap, the profile of the ablated area matches with the truncated Gaussian profile of the laser beam, and localized surface roughness in the ablated region is ~ 50 nm, based on the ripples in the majority of the depth profile. Since only a small fraction of the total energy of 20 mJ available from the laser was used for the ablation, with suitable laser spot

size and scan parameters, the scan time can be reduced significantly. Furthermore, shaping of the laser beam profile is expected to result in more uniform ablation. The ablation depth is comparable for the single crystal diamond also. However, preliminary crystallography measurements of this single crystal sample show that although the peak position of the diffraction signal is unaltered, line width is broader in the ablated region, indicating the introduction of stress/strain in the crystal after ablation.

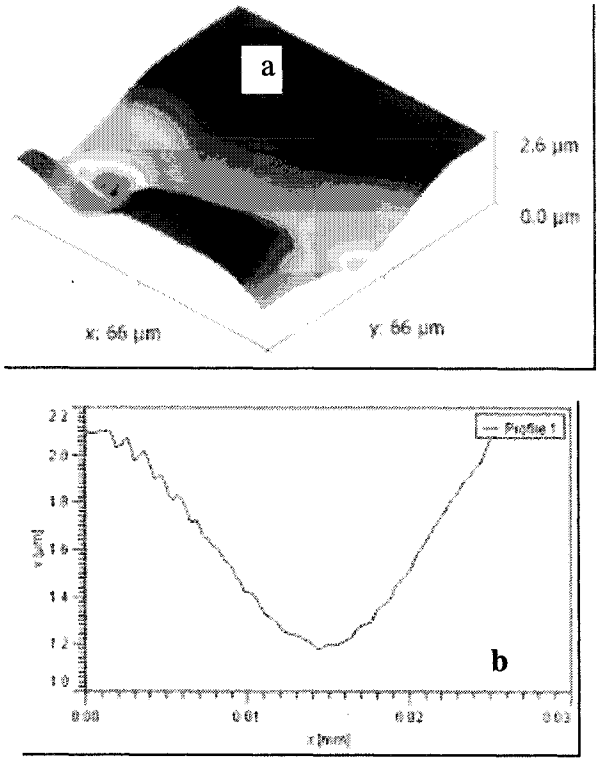

Figure 7 AFM picture (a) and depth profile (b) of the ablated region of the polycrystalline diamond

Inductively coupled plasma reactive ion etching (ICPRIE):

A small section of one of the one cm diameter polycrystalline samples was laser ablated and then sent to Diamonex for reactive ion etching. A second sample was etched in house with following parameters: Power (ICP) = 800 W, Power (RF) = 15 W, etching gases of O_2 and Ar with oxygen flow of 40 sccm., etch rate of 65 nm/minute, and etch time of 45 minutes resulting in an etched depth of 3 µm. Argon flow is varied (typically up to 20% of oxygen flow). An SEM picture of the etched and masked surfaces of this sample is shown in Figure 8 and the AFM picture of the commercially etched sample is shown in Figure 9. Both these figures indicate that reactive ion etching results in a smooth surface. Preliminary crystallography measurements on single crystal diamond do not show any change in the crystal structure due to RIE. The final process for the capsule may involve laser ablation for significant thinning of the diamond, followed by RIE for smoothing the surface and removing the stressed layers.

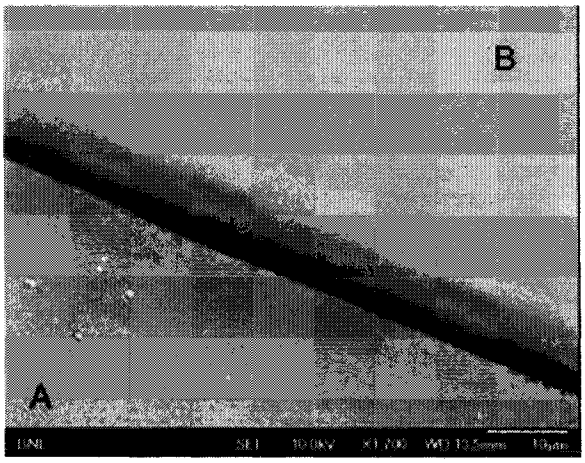

Figure 8 SEM picture of reactive ion etched (A) and protected (B) polycrystalline diamond

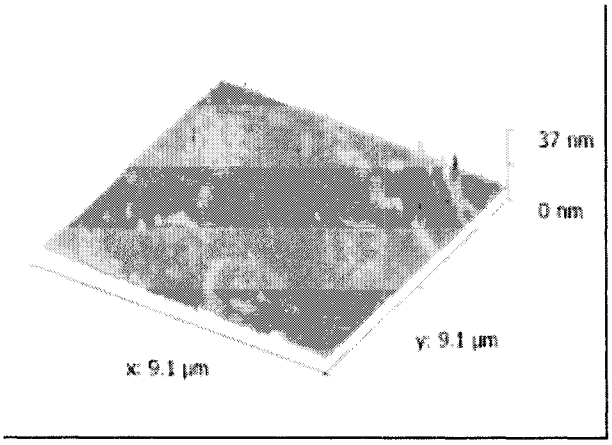

Figure 9 AFM picture of polycrystalline diamond reactive ion etched by Diamonex. Note the vertical scale is in nm while the x and y scales are in µm.

SIMULATION OF ELECTRON TRANSPORT IN DIAMOND

Secondary electron generation and elastic scattering within diamond have been simulated using Monte Carlo models within VORPAL PIC code by Tech-X. The secondary electron yield for a variety of primary electron energies, and the time evolution of spatial and energy distribution of the secondary electrons have been calculated. Preliminary results indicate that gains of up to two orders of magnitude are possible with a few keV primary electrons, electron-electron scattering narrows the energy distribution of secondary electrons to a few tens of eV within 100 fs and during this time, the spatial distribution evolves to be spherically uniform, extending over ~ 25 nm radius. In these simulations, electron-phonon interaction, charge-impurity scattering, electron-hole recombination and the effect of the applied field and temperature in the transport have not been included, but will be incorporated in future simulations.

ACKNOWLEDGEMENT

The authors would like to acknowledge the expert technical assistance by J. Walsh, W. Smith and D. Pate. AI would like to acknowledge the early support from K. Evans-Lutterodtin the RIE processes. The IR transmission measurements were done using the U2B IR beamline at the NSLS, administered by the Center for Synchrotron Biosciences, Case Western Reserve University, supported by the National Institute for Biomedical Imaging and Bioengineering under P41-EB-01979. This manuscript has been authored by Brookhaven Science Associates, LLC under Contract No. DE-AC02-98CH10886 with the U.S. Department of Energy. The United States Government retains, and the publisher, by accepting the article for publication, acknowledges, a world-wide license to publish or reproduce the published form of this manuscript, or allow others to do so, for the United States Government purposes.

REFERENCES

[1] Litvinenko V. N., Beavis D., et al. "High Current Energy Recovery Linac at BNL", Proc. of PAC 05, Knoxville TN, p 2242

[2] Ben-Zvi I., Brennan J., et al. "R&D towards cooling of the RHIC Collider" NIM A 532 (2004) 177

[3] Workshop on Photo-injector for Energy Recovery Linac, January 22 & 23, 2001 Brookhaven National Laboratory , Upton, NY, BNL Report 52624

[4] I. Ben-Zvi, T. Rao et.al. "Diamond secondary emitter" presented at ICFA Workshop on the Physics and Applications of High Brightness Electron Beams, Oct. 2005, Erice, Italy

[5] Yater J. E. and Shih A, "Secondary electron emission characteristics of single-crystal and polycrystalline diamond", J. Appl. Phys., 87, (2000) 8103

[6] Watanabe T., Teraji T., et al. "Monte Carlo simulations of electron transport properties of diamond in high electric fields using full band structure", J. Appl. Phys. 95 (2004) 4866

[7] George T., Foote M. C., et al. "Below band gap laser ablation of diamond for transmission electron microscopy" Appl. Phys Lett. 62, (1993) 2880